

Assessment of thoracic spinal cord electrophysiological activity through magnetoneurography



Jun Hashimoto^a, Shigenori Kawabata^{a,b,*}, Toru Sasaki^a, Yuko Hoshino^b, Kensuke Sekihara^b, Yoshiaki Adachi^c, Taishi Watanabe^d, Yuki Miyano^d, Yuki Mitani^d, Shinji Sato^d, Sukchan Kim^d, Toshitaka Yoshii^a, Atsushi Okawa^a

^a Department of Orthopaedic Surgery, Graduate School of Medical and Dental Sciences, Tokyo Medical and Dental University, 1-5-45 Yushima, Bunkyo-ku, Tokyo 113-8510, Japan

^b Department of Advanced Technology in Medicine, Graduate School of Medical and Dental Sciences, Tokyo Medical and Dental University, 1-5-45 Yushima, Bunkyo-ku, Tokyo 113-8510, Japan

^c Applied Electronics Laboratory, Kanazawa Institute of Technology, 3 Amaike-cho, Kanazawa City, Ishikawa 920-1331, Japan

^d RICOH Company, Ltd., 1-3-6 Nakamagome, Ohta-ku, Tokyo 143-8555, Japan

ARTICLE INFO

Article history:

Accepted 30 September 2021

Available online 5 November 2021

Keywords:

Magnetoneurography

Magneto-spinography

Thoracic myelopathy

Spinal cord

Electrophysiological activity

Sciatic nerve stimulation

HIGHLIGHTS

- The biomagnetic field around the current flowing in the thoracic spinal cord was measured by a magnetoneurograph system.
- Our novel method for synchronized bilateral sciatic nerve stimulation obtained an adequate magnetic signal for assessment.
- This is the first report to achieve noninvasive and detailed visualization of thoracic electrophysiological activity.

ABSTRACT

Objective: Noninvasive and detailed visualization of electrophysiological activity in the thoracic spinal cord through magnetoneurography.

Methods: In five healthy volunteers, magnetic fields around current flowing in the thoracic spinal cord after alternating unilateral and synchronized bilateral sciatic nerve stimulation were measured using a magnetoneurograph system with superconductive quantum interference device biomagnetometers. The current distribution was obtained from the magnetic data by spatial filtering and visualized by superimposing it on the X-ray image. Conduction velocity was calculated using the peak latency of the current waveforms.

Results: A sufficiently high magnetic signal intensity and signal-to-noise ratio were obtained in all participants after synchronized bilateral sciatic nerve stimulation. Leading and trailing components along the spinal canal and inward components flowing into the depolarization site ascended to the upper thoracic spine. Conduction velocity of the inward current in the whole thoracic spine was 42.4 m/s.

Conclusions: Visualization of electrophysiological activity in the thoracic spinal cord was achieved through magnetoneurography and a new method for synchronized bilateral sciatic nerve stimulation. Magnetoneurography is expected to be a useful modality in functional assessment of thoracic myelopathy.

Significance: This is the first report to use magnetoneurography to noninvasively visualize electrophysiological activity in the thoracic spinal cord in detail.

© 2021 International Federation of Clinical Neurophysiology. Published by Elsevier B.V. This is an open access article under the CC BY license (<http://creativecommons.org/licenses/by/4.0/>).

Abbreviations: MNG, magnetoneurography; MRI, magnetic resonance imaging; OPLL, ossification of the posterior longitudinal ligament; SCEP, spinal cord evoked potential; SEP, somatosensory evoked potential; SNR, signal-to-noise ratio; SQUID, superconductive quantum interference device.

* Corresponding author at: Department of Advanced Technology in Medicine, Graduate School of Medical and Dental Sciences, Tokyo Medical and Dental University, 1-5-45 Yushima, Bunkyo-ku, Tokyo 113-8510, Japan.

E-mail addresses: hash.orth@tmd.ac.jp (J. Hashimoto), kawabata.orth@tmd.ac.jp (S. Kawabata), t-sasaki.orth@tmd.ac.jp (T. Sasaki), hoshino.atm@tmd.ac.jp (Y. Hoshino), k-sekihara@nifty.com (K. Sekihara), adachi@ael.kanazawa-it.ac.jp (Y. Adachi), taishi.watanabe@jp.ricoh.com (T. Watanabe), yuki.yh.hasegawa@jp.ricoh.com (Y. Miyano), yuuki.ym.mitani@jp.ricoh.com (Y. Mitani), shinji.s1.sato@jp.ricoh.com (S. Sato), sukchan.kim@jp.ricoh.com (S. Kim), yoshii.orth@tmd.ac.jp (T. Yoshii), okawa.orth@tmd.ac.jp (A. Okawa).

<https://doi.org/10.1016/j.clinph.2021.09.023>

1388-2457/© 2021 International Federation of Clinical Neurophysiology. Published by Elsevier B.V. This is an open access article under the CC BY license (<http://creativecommons.org/licenses/by/4.0/>).

1. Introduction

Thoracic myelopathy causes severe symptoms, such as back pain, numbness of the lower extremity, gait disturbance, and bowel and bladder dysfunction. Although its surgical treatment is effective (Aizawa et al., 2007, Matsuyama et al., 2005), reported risk factors for a poor surgical outcome include a longer preoperative duration of symptoms, worse preoperative symptoms, and ossification of the posterior longitudinal ligament (OPLL) (Aizawa et al., 2007, Onishi et al., 2016). Early and precise diagnosis of thoracic myelopathy is essential, but difficult. For instance, thoracic myelopathy often occurs simultaneously with cervical myelopathy and lumbar spinal canal stenosis and can be overlooked (Hsieh et al., 2014, Shields et al., 2019). Furthermore, OPLL develops at multiple spinal levels, complicating identification of the responsible lesion.

Diagnosis of thoracic myelopathy requires both morphological and functional assessment. Magnetic resonance imaging (MRI) is useful and widely used for obtaining morphological information, such as cord compression and intracord signal changes. However, not all cases of thoracic myelopathy have clinical symptoms (Kato et al., 2012, Matsumoto et al., 1998). Physical and neurological examinations as basic functional assessment methods are unable to identify a detailed responsible lesion because there are no deep tendon reflex and manual muscle tests specific to each level in the thoracic spine, unlike in the cervical and lumbar spine. Furthermore, comorbid lumbar spinal stenosis often interferes with the functional assessment due to the similarity of their symptoms (Hsieh et al., 2014). Although electrophysiological testing including somatosensory evoked potentials (SEPs) is additionally performed, the signal is weaker in the spinal cord than in the peripheral nerves because of its depth from the body surface (Kakigi et al., 1982, Yamada et al., 1982). Detailed measurement of spinal cord evoked potentials (SCEPs) requires epidural electrodes, which are useful but invasive (Shinomiya et al., 1988, Tani et al., 2000). Therefore, noninvasive and detailed electrophysiological testing is necessary.

We have developed a magnetoneurography (MNG) system that can noninvasively assess the neurophysiological activity of the spinal cord and the peripheral nerves by measuring the magnetic fields around the neural current. It is based on the principle that magnetic fields are barely influenced by the surrounding tissue, which includes bone, muscle, and cerebrospinal fluid (Trahms et al., 1989). Highly sensitive magnetic sensors (Adachi et al., 2017) enable us to measure the biomagnetic signals around the spinal cord, which are just 10^{-9} of those of the geomagnetic field (Wijesinghe, 2010). Moreover, the current distribution is obtained from the magnetic signals, and the currents, including intra-axonal currents and inward currents flowing into the depolarization site (Noble, 1966), are observed with high spatial resolution.

In our previous studies, MNG was used to visualize electrophysiological activity in the spinal cord of animals (Fukuoka et al., 2004, Fukuoka et al., 2002, Hoshino et al., 2005, Kawabata et al., 2002, Ohkubo et al., 2003, Sakaki et al., 2020, Tomizawa et al., 2008, Tomori et al., 2010). Furthermore, the electrophysiological activity in the cervical spinal cord of healthy volunteers was measured after peripheral nerve stimulation (Sumiya et al., 2017), whereas that in the cauda equina was measured after tibial nerve and peroneal nerve stimulation (Ishii et al., 2012, Ushio et al., 2019). However, visualization of thoracic electrophysiological activity was not achieved because the signal obtained by percutaneous stimulation of the peroneal or tibial nerve was too weak. The aim of this study was thus to noninvasively visualize thoracic electrophysiological activity through MNG by using a novel method, synchronized bilateral sciatic nerve stimulation.

2. Materials and methods

2.1. Participants

The study protocol was approved by the institutional review board of Tokyo Medical and Dental University Medical Hospital. Written informed consent was obtained from all participants. This study included five healthy volunteers without neurological symptoms or abnormal findings on thoracic and lumbar spinal MRI. They were all men aged 28–45 years (mean, 34.6 years) with a mean body mass index of 20.9 kg/m².

2.2. MNG system

In a magnetically shielded room, biomagnetic fields were measured with a 132-channel superconductive quantum interference device (SQUID) biomagnetometer developed with Kanazawa Institute of Technology and RICOH Company, Ltd. (Fig. 1) (Adachi et al., 2017). The biomagnetometer contains 44 cylindrically shaped SQUID sensors in an area of 130 × 180 mm (Fig. 2a). Each sensor measures magnetic fields in three orthogonal directions to obtain three-dimensional biomagnetic information. The X, Y, and Z directions were set from the left to right, from the caudal to cranial, and from the ventral to dorsal of the body in the positive direction, respectively (Fig. 2b).

2.3. Measurement

Participants were placed in a relaxed supine position with their thoracic or lumbar back on the sensors (Fig. 3). Frontal and lateral X-rays obtained the positional information between the body and sensors through marker coils set at the four corners. The bilateral sciatic nerves were electrically stimulated at the proximal popliteal fossa (square wave pulse; 5 Hz in frequency; 0.3 ms in duration) by an MEE system (Nihon Kohden Company, Tokyo, Japan). The cathode and anode of the sealed surface electrodes were placed over the proximal popliteal fossa and the patellar tendon, respectively. Supramaximal stimulation (1.2 times as strong as the maximal compound motor action potentials) was performed while the system monitored the compound muscle action potentials of both the abductor hallucis muscle and extensor digitorum brevis muscle.

Evoked magnetic fields from the lumbar to upper thoracic spine in response to alternating unilateral and simultaneous bilateral sciatic nerve stimulation were measured by shifting the measurement areas several times under the following conditions: sampling rate, 40 kHz; band-pass filter, 100–5000 Hz; averaging 2000 times in the lumbar area, 4000 times in the lower thoracic area, and 8000 times in the middle to upper thoracic areas. The dual signal subspace projection method reduced artifact noise related to electrical stimulation (Sekihara et al., 2016). The intensity of the signal was defined as the maximum baseline-to-peak amplitude, whereas that of the noise was defined as the root mean square of the values 0–5 ms before the stimulation. The signal-to-noise ratio (SNR) value was calculated by dividing the maximum baseline-to-peak amplitude by the noise. The measurement was considered reliable if the SNR value was 3 or more. The magnetic signal intensity and SNR value were statistically compared after unilateral (average of left and right) and bilateral sciatic nerve stimulation by paired t-test after normality was examined by the Shapiro-Wilk normality test. A P value less than 0.05 was considered statistically significant.

Unit gain constraint recursively applied null-steering spatial filtering obtained the current temporal distribution from the magnetic data (Kumihashi and Sekihara, 2010, Sekihara and Nagarajan, 2015). The current distribution at the depth of the



Fig. 1. Appearance of the magnetoneurography system in a magnetically shielded room. A customized bed was placed in the center of the room, and a smaller box with SQUID sensors (a) was set on the same plane as that of the bed. The dotted square indicates the sensor area. The box with sensors protruded from a cryostat box (b), which refrigerated the sensors with liquefied helium to maintain superconducting conditions. Two irradiating devices were set to check the positional relationship between the sensors and the participant's measurement area from the frontal (c) and lateral (d) views. SQUID, superconductive quantum interference device.

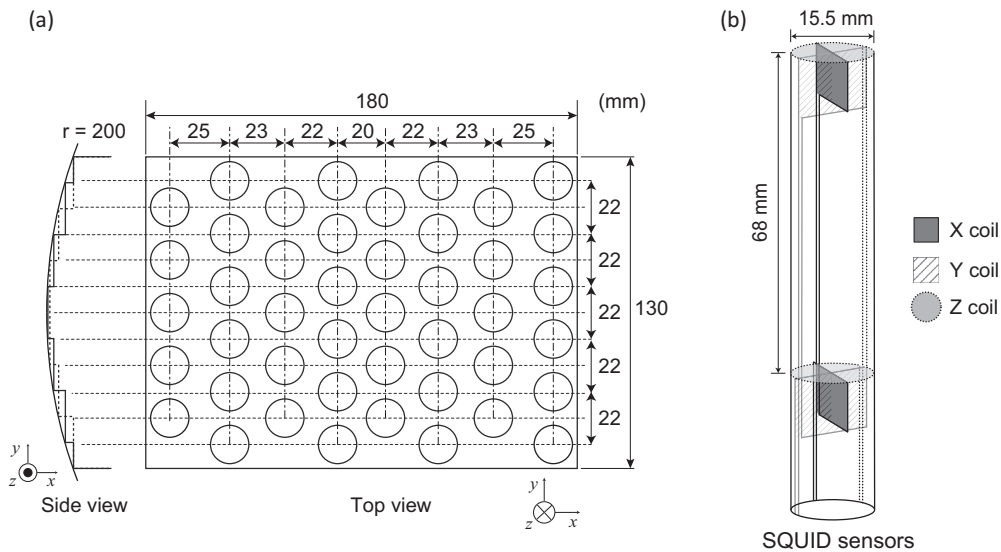


Fig. 2. An array of SQUID sensors. A total of 44 SQUID sensors are arranged in a 180 mm × 130 mm area along a rounded surface (a) in the box shown in Fig. 1(a). Each sensor (b) measured three orthogonal directional magnetic fields via X, Y, and Z coils. SQUID, superconductive quantum interference device.

spinal canal was visualized by its superimposition on the frontal X-ray. Moreover, the current waveforms flowing in the spinal canal were obtained using a “virtual electrode”, which can be placed anywhere to obtain the current waveform. The conduction velocities were calculated from the peak latencies and the distance obtained by the X-rays.

2.4. Novel stimulation method

We developed a method for synchronized bilateral sciatic nerve stimulation to obtain much stronger currents (Fig. 4). First, the current distribution of the lumbar spinal area was measured after

alternating bilateral sciatic nerve stimulation. Second, we calculated each peak latency of the inward currents reaching the center of the L3 vertebra, where the caudal equina, including the sciatic nerve component, is found in the spinal canal. Third, the timing of the stimulation was shifted by the difference in peak latency so that the bilateral current reached the L3 vertebra at the same time.

3. Results

We measured the evoked magnetic fields of the lumbar and thoracic spinal area in response to alternating unilateral and syn-



Fig. 3. Lateral view of the sensors and subject. The subject lay on the bed in a relaxed supine position and placed his back on the sensors. The bilateral sciatic nerves were stimulated at the proximal popliteal fossa.

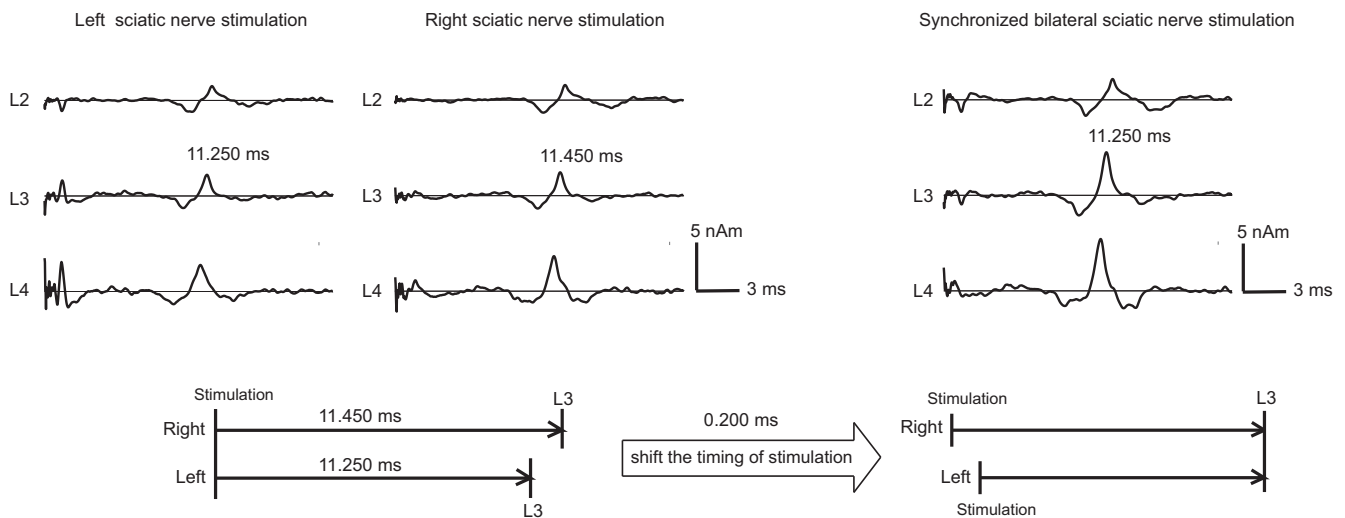


Fig. 4. Synchronized bilateral sciatic nerve stimulation. The peak latencies of the inward currents at the center of the L3 vertebra were 11.250 and 11.450 ms after left and right sciatic nerve stimulation, respectively. The inward currents were adjusted so that they reached the L3 vertebra at the same time by shifting the timing of the stimulation by the difference in the peak latency (0.200 ms).

chronized bilateral sciatic nerve stimulation in all participants. Table 1 shows the magnetic signal intensity and SNR value in the caudal direction at the L2, T10, T6, and T2 vertebra levels along the spinal column for the X-coils after left, right, and bilateral stimulation, reflecting the magnetic field intensity around the trailing component of intra-axonal current. Both the magnetic signal intensity and SNR value in each participant decreased at more cranial areas due to temporal dispersion after unilateral and bilateral sciatic nerve stimulation. Synchronized bilateral sciatic nerve stimulation resulted in a significantly higher magnetic signal intensity and SNR value in the lumbar, lower thoracic, and middle thoracic spinal area than unilateral stimulation (paired t-test, all P values < 0.05). In most measurements, the magnetic signal intensity after bilateral sciatic nerve stimulation was almost the same as the sum of those after left and right sciatic nerve stimulation, but differed in some measurements at cranial region. In synchronized

bilateral sciatic nerve stimulation, the left and right stimulation timing was shifted by 0.1 or 0.2 ms for each participant. The data from cases 2 and 3 were not considered reliable because the SNR values were less than 3 in the measurement of the upper thoracic spinal area after unilateral sciatic nerve stimulation.

The magnetic waveforms at the mid-thoracic spinal area after bilateral sciatic nerve stimulation in a representative 35-year-old man are shown in Fig. 5. The X-directional waveforms increased in peak latency at more cranial areas. In other words, they traveled to the cranial area along the thoracic spine. The Y- and Z-directional waveforms had opposite polarities on the bilateral sides to the spinal column and traveled to the cranial area bilaterally 30–60 mm away from the spine.

The evoked current distribution in the lumbar and thoracic spinal areas after bilateral sciatic nerve stimulation was visualized as a pseudo-color map including the intensity and vector of the

Table 1 Participants' demographic characteristics, magnetic signal intensity, signal-to-noise ratio, and how far the current conducted after unilateral and bilateral sciatic nerve stimulation by magnetoneurography.

Case	Age, years	Sex	Body height, cm	Body weight, kg	BMI, kg/m ²	Magnetic signal, fT (Signal-to-noise ratio)						How far the current conducted				
						L2		T10		T6		T2		Uni. Stim.	Bil. Stim.	
						Uni. Stim.	Bil. Stim.	Uni. Stim.	Bil. Stim.	Uni. Stim.	Bil. Stim.	Uni. Stim.	Bil. Stim.			
1	35	male	169	56	19.6	Left	82.3 (16.0)	148 (25.1)	24.3 (9.2)	38.1 (16.1)	8.2 (4.4)	20.6 (7.7)	4.9 (1.9)	12.2 (5.7)	T5	T1
						Right	62.3 (18.1)	14.8 (5.5)	14.8 (5.5)	9.0 (5.0)	9.0 (5.0)	5.9 (3.8)	5.9 (3.8)	5.9 (3.8)	5.9 (3.8)	
2	28	male	176	57	18.4	Left	87.4 (13.7)	198 (23.5)	20.2 (8.0)	31.3 (11.5)	7.0 (3.2)	18.9 (8.9)	-	11.0 (5.2)	T5	T1
						Right	98.5 (12.5)	15.0 (4.4)	15.0 (4.4)	7.4 (3.2)	7.4 (3.2)	-	-	-	-	
3	45	male	163	60	22.6	Left	88.0 (19.6)	155 (26.8)	18.3 (6.2)	37.3 (12.4)	16.4 (6.5)	28.5 (9.4)	-	14.8 (5.1)	T6	T1
						Right	88.6 (19.1)	21.4 (7.1)	21.4 (7.1)	12.7 (4.8)	12.7 (4.8)	-	-	-	-	
4	32	male	183	78	23.3	Left	78.4 (11.3)	166 (21.1)	16.5 (6.0)	34.5 (10.7)	8.8 (4.0)	23.0 (7.8)	7.5 (3.0)	13.1 (5.7)	T5	T1
						Right	94.1 (16.3)	17.1 (5.7)	17.1 (5.7)	9.0 (5.1)	9.0 (5.1)	4.5 (1.6)	4.5 (1.6)	4.5 (1.6)	4.5 (1.6)	
5	33	male	163	55	20.7	Left	82.8 (10.6)	191 (27.8)	17.8 (5.7)	38.4 (15.4)	10.3 (4.2)	18.5 (7.7)	8.5 (4.0)	14.0 (5.3)	T5	T1
						Right	106 (12.0)	19.3 (7.0)	19.3 (7.0)	7.9 (3.8)	7.9 (3.8)	7.1 (3.4)	7.1 (3.4)	7.1 (3.4)	7.1 (3.4)	
mean	34.6		171	61	20.9	86.8 (14.9)	172 (24.9)	18.5 (6.5)	35.9 (13.2)	9.7 (4.4)	21.9 (8.3)	6.4 (2.5)	13.0 (5.4)			

BMI, body mass index; Uni. Stim., Unilateral sciatic nerve stimulation; Bil. Stim., Bilateral sciatic nerve stimulation.

current and was superimposed on the frontal X-ray (Fig. 6). Three kinds of current components propagated as a group from the lumbar region to the upper thoracic spine. First, the leading current components with a cranial vector flowed along the spine. Second, the inward current components directing orthogonally to the spinal canal flowed bilaterally 30–60 mm lateral to the spine. Finally, the trailing current components with a caudal vector followed them along the spine. The inward currents reached the L3 level 10.5 ms after bilateral sciatic nerve stimulation, and their grouped currents traveled to the cranial direction over time. The currents could be seen in the upper thoracic spinal area, although the current intensity decreased at the more cranial area due to temporal dispersion. A movie detailing the current distribution is shown in Video 1. A group of currents propagated to the lower thoracic spine and seemed to disappear at 11 ms and reappear. Then, the currents flowed to the upper thoracic spine. **Video 1**.

These current components were also presented as the current waveforms obtained by “virtual electrodes”. The leading and trailing intra-axonal components were confirmed as the upward and downward traveling currents, respectively in Fig. 7a-c, and the inward components were confirmed as the upward traveling currents in Fig. 7d-f. Their current waveforms gradually increased in peak latency and decreased in amplitude at more cranial areas. The waveforms after synchronized bilateral sciatic nerve stimulation were close to the combined waveforms after right and left stimulation, except in the thoracolumbar region where the waveforms were complicated. Consequently, the currents conducted to more cranial areas after bilateral sciatic nerve stimulation than those after unilateral stimulation. **Table 1** shows how far the inward currents conducted to the cranial area with a SNR exceeding 3 in each participant. Although the inward currents after unilateral sciatic nerve stimulation conducted only to the middle thoracic area, those after bilateral stimulation conducted to T1 in all participants.

Table 2 shows the peak latency and the conduction velocity of the inward currents in the lumbar and thoracic spinal area after bilateral sciatic nerve stimulation in each participant. The conduction velocity of the inward current in the whole thoracic spine after bilateral sciatic nerve stimulation was 42.4 ± 3.5 m/s, which was calculated by dividing the distance from the T12 to T1 vertebrae on X-ray by the peak latency difference of the inward current. Inversely, the conduction velocity in the lumbar spine was 82.7 ± 6.1 m/s.

4. Discussion

Here, we successfully visualized the electrophysiological activity of the thoracic spinal cord with MNG. SEPs from the body surface cannot be evaluated in detail and need a high skill level to minimize noise (Cracco, 1973, Kakigi et al., 1982, Yamada et al., 1982). On the other hand, epidural SCEPs obtain detailed information but are invasive and difficult to perform (Jones et al., 1982, Macon and Poletti, 1982). As a result, these methods are not widespread. To the best of our knowledge, we are the first to conduct noninvasive and detailed functional assessment of the thoracic spinal cord. This was possible because our novel method for synchronized bilateral sciatic nerve stimulation obtained a sufficiently high magnetic signal intensity and SNR value. In our previous study, the magnetic signal intensity of the lumbar spinal area after unilateral peroneal nerve stimulation had a peak-to-peak amplitude of 60 fT (Ushio et al., 2019). In the present study, however, the magnetic signal intensity after synchronized bilateral sciatic

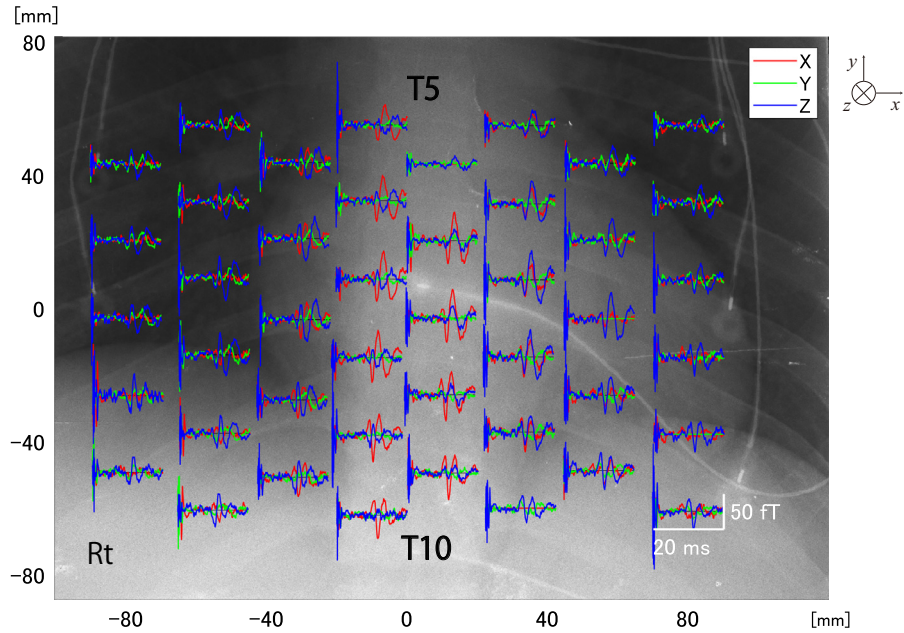


Fig. 5. Magnetic fields on each sensor and X-ray image. The magnetic fields measured using 44 sensors are represented as time on the horizontal axis and magnetic signal intensity on the vertical axis and are superimposed on the frontal X-ray of the mid-thoracic spinal area. Moreover, three directional magnetic fields (X, Y and Z axes) are superimposed on each sensor. The X, Y, and Z directions are set positive from the left to right, from the caudal to cranial, and from the dorsal to ventral of the body, respectively.

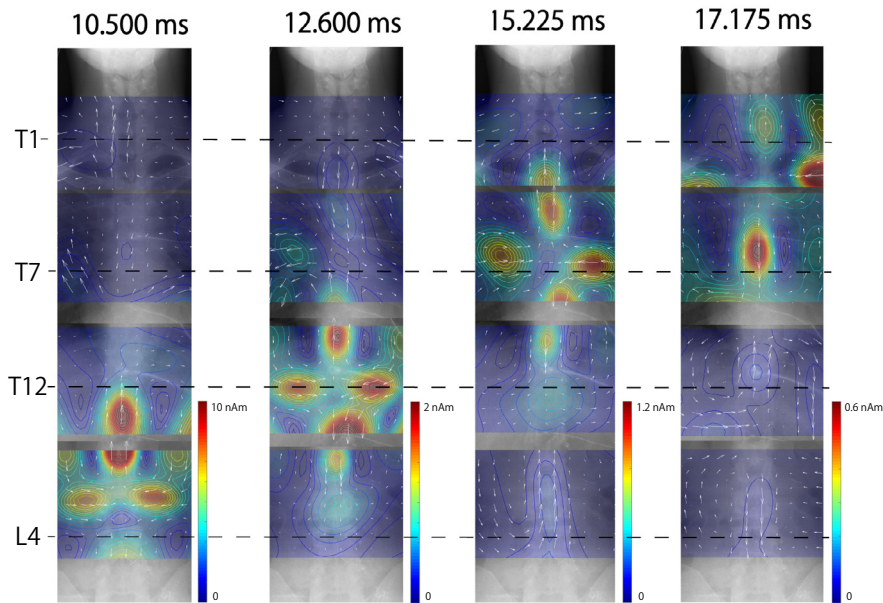


Fig. 6. Current distribution after synchronized bilateral sciatic nerve stimulation in a representative case of a 35-year-old male. The current distribution is superimposed on the frontal X-ray image and arranged from the lumbar to upper thoracic spinal area along the time course. White arrows indicate the direction of the current at each point, and the color indicates the intensity: red is strong and blue is weak. The leading component flowed into the L1, T10, T5, and C7 levels at 10.500, 12.600, 15.225, and 17.175 ms after stimulation, respectively. Similarly, the inward components, which are bilaterally perpendicular to the spinal canal, and the trailing components with a caudal vector follow the leading component. The leading, inward, and trailing components flow to the upper thoracic spine as one group. In this figure, the current intensity becomes smaller at more cranial areas due to temporal dispersion, and the color scale is changed to improve its visualization.

nerve stimulation was much higher, 172 ft, even though it was expressed as baseline-to-peak amplitude which is approximately half of peak-to-peak amplitude.

There are three possible reasons why a much higher signal intensity and SNR value were obtained. First, stimulation of the sciatic nerve including not only the peroneal, but also the tibial nerve branch, involved more nerve fibers. Second, we stimulated the sciatic nerve at the proximal popliteal fossa where it is more proximal

than the peroneal head during peroneal nerve stimulation. The stimulus point was shifted proximally, reducing temporal dispersion, in which currents gradually decay with conduction. Finally, and most importantly, our novel approach to synchronized bilateral sciatic nerve stimulation succeeded in obtaining a much higher signal intensity. Inward currents with sufficient SNR value conducted only to the middle thoracic spinal area after unilateral sciatic nerve stimulation but through the whole thoracic spinal

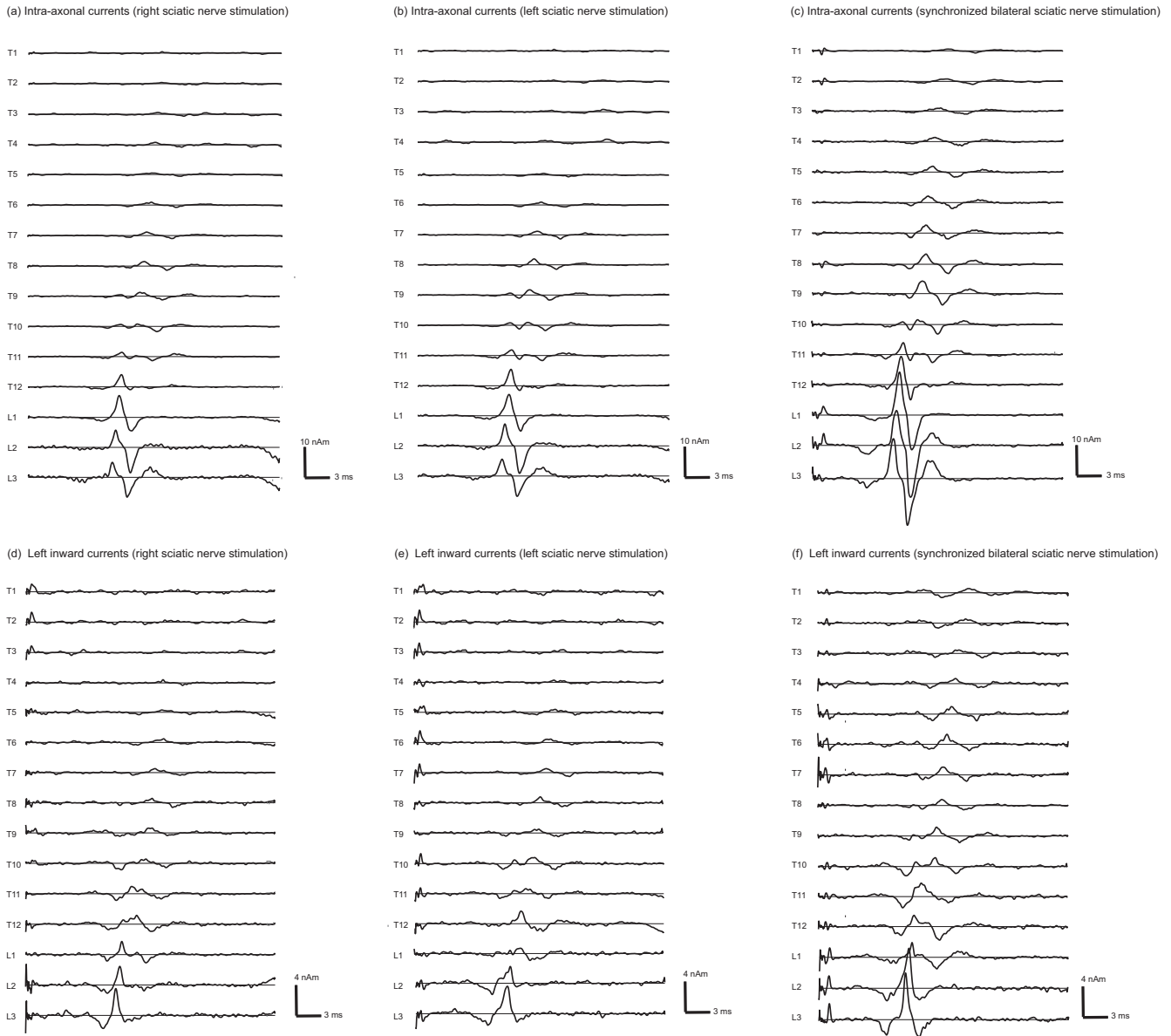


Fig. 7. Current waveforms in the thoracic and lumbar spine after unilateral and bilateral sciatic nerve stimulation. The current waveforms in (a), (b), and (c) are obtained from the virtual electrodes set on the center of each vertebra from L3 to T1 after right, left, and bilateral sciatic nerve stimulation, respectively. The upward direction of the waveform is the cranial direction. The leading and trailing intra-axonal components are confirmed as the positive peak at 10 ms and the negative peak at 11.5 ms at the L3 level, respectively. Their current waveforms gradually increase in peak latency in more cranial areas and travel from the lumbar to thoracic spinal area. In (d), (e), and (f), the current waveforms for the inward components are obtained from virtual electrodes set 35 mm left from the center of each vertebra after right, left, and bilateral sciatic nerve stimulation, respectively. The upward direction of the waveforms is the direction perpendicular to the spinal canal. The inward components are observed as the positive peak at 10.5 ms at the L3 level. Waves traveling from the lumbar to thoracic spine are observed.

Table 2
Participants' functional characteristics measured by magnetoneurography.

Case	Peak latency, ms				Conduction velocity, m/s			
	L3	T12	T7	T1	L3-L1	T12-T10	T7-T3	T12-T1
1	10.43	12.46	14.93	18.30	83.9	40.0	44.9	44.9
2	11.25	12.83	16.94	18.90	80.0	30.0	49.7	38.0
3	10.35	12.33	14.85	18.34	75.2	33.5	48.1	41.6
4	11.39	12.99	15.91	18.94	82.5	37.0	50.3	46.9
5	10.13	11.68	14.63	17.76	91.9	34.1	41.7	40.7
Mean	10.71	12.46	15.45	18.45	82.7	34.9	46.9	42.4

area after synchronized bilateral sciatic nerve stimulation. The stimulation timing was shifted by 0.1 or 0.2 ms in every participant to match the timing of the bilateral current entries into the spinal

cord because the points used to stimulate both the peroneal and tibial branches with supramaximal intensity often differ between the left and right sides. Consequently, the magnetic signal intensi-

ties after synchronized bilateral sciatic nerve stimulation obtained almost the same as the sum of those after left and right stimulation in the lumbar and lower thoracic region. However, some measurements in the middle thoracic region did not show similar results because the interactive effect of the facilitation or inhibition between the currents after left and right stimulation could not be eliminated due to the increased variability by temporal dispersion. In addition, the inward currents in the thoracolumbar region after bilateral stimulation were different from the combined current after left and right stimulation because the neural activity may be complicated where the caudal nerve enters the spinal cord.

Traveling current waveforms in the lumbar and thoracic spine were observed after synchronized bilateral sciatic nerve stimulation and, interestingly, the conduction velocities in the thoracic and lumbar spine were very different at 42.4 and 82.7 m/s, respectively. This result is similar to that of a previous SEP study (Cracco, 1973) and indicates that the mainly observed components were different between the lumbar and thoracic spine. The faster wave in the lumbar spine may be due to retrograde conduction in the motor nerve or conduction through group Ia muscle afferent fibers because more motor nerves were stimulated by supramaximal stimulation in compound motor action potentials. Moreover, because the faster wave stopped propagating at the lower thoracic spine, a component represented as F wave or H wave may be observed.

An epidural SCEP study during scoliosis surgery revealed that several currents with different speeds propagated in the thoracic spine (Jones et al., 1982); the faster current ascends in the spinocerebellar tract from the peripheral nerves through group Ia afferent muscle fibers while the slower current ascends in the dorsal column. On the other hand, SEPs from the body surface are reported to be unable to clearly separate their two components (Cracco, 1973). The slower wave propagating in the thoracic spine in this study is probably derived from components ascending in the dorsal column, although we cannot exclude the possibility that several components were mixed. Regarding conduction velocity, spinal SEPs measured from the body surface after peripheral nerve stimulation showed that the ascending current propagated at about 50–70 m/s in the thoracic spine (Cracco, 1973, Desmedt and Cheron, 1983, el-Negamy and Sedgwick, 1978, Jones et al., 1982, Kakigi et al., 1982, Schiff et al., 1984, Yamada et al., 1982), which is faster than in the present study. This dissociation may arise from how distances and latencies are measured. The distance of the spinal cord was measured on the body surface in previous studies, and it was possibly overestimated because of the spinal curvature (thoracic kyphosis) (Desmedt and Cheron, 1983). In other words, the actual conduction velocity may be slower. However, in this study, a more accurate distance was obtained through frontal and lateral X-rays that included spinal curvature information. Moreover, we adopted peak latency, related to the most numerous components, not onset latency, used by most previous studies and related to the fastest components. Therefore, the conduction velocity in this study may be slower.

Conduction velocity was clearly altered in the lower thoracic spine. The possible reason is that complex branching and synaptic transfer occurs at the entry zone of the spinal cord. In previous studies of SEPs from the body surface, the amplitude was highest there because pre- and postsynaptic fibers concentrate at the conus medullaris (Cracco, 1973, Desmedt and Cheron, 1983, Kakigi et al., 1982, Maccabee et al., 1983), with epidural SEPs revealing that the conduction velocity decreased to about 30 m/s due to synapsing (Jones et al., 1982, Lloyd and McIntyre, 1950, Macon and Poletti, 1982). In the present study, the current waveforms, presented as a representative case in Fig. 7c, f, also showed that the current amplitude was the highest in the upper lumbar region and that the mean conduction velocity was 34.9 m/s in

the T10–12 spinal area (Table 2). In addition, detailed visualization of the current distribution by MNG showed that the ascending currents seemed to disappear and appear again at the lower thoracic spine (Video 1). One possible reason is that ascending currents may cancel each other out due to complex branching and synapsing when they enter the spinal cord. In addition, MNG calculated evoked currents from the magnetic signals, not actual currents, and magnetic signals with opposite vectors cancel each other out and make it seem that there is no current. Another possible reason is that MNG may be unable to detect the magnetic fields rising from the current flowing from the dorsal to the ventral direction because MNG measures from the dorsal direction. Our next step is to investigate the electrophysiological activity of the lower thoracic spine.

This study has several limitations. First, a small number of participants were analyzed. Second, relatively young volunteers were enrolled, and further study of elderly individuals, who are more likely to have thoracic myelopathy and similar conditions, is needed. Measurement in a more diverse and larger population will allow us to determine the normal range of the conduction velocity according to age and permit accurate assessment of spinal cord function. Third, the electrophysiological activity in the conus medullaris is not yet understood. This will be our next research topic.

In conclusion, MNG permitted visualization of the electrophysiological activity in the thoracic spinal cord via a novel method for synchronized bilateral sciatic nerve stimulation. MNG is expected to be a useful modality for the functional assessment of thoracic myelopathy.

Funding

This research was supported by RICOH Company. The funding body played no role in study design, data collection and analysis, preparation of the manuscript, or the decision to publish.

Declaration of Competing Interest

The authors declare that they have no known competing financial interests or personal relationships that could have appeared to influence the work reported in this paper.

References

- Adachi Y, Kawabata S, Fujihira J-I, Uehara G. Multi-channel SQUID magnetospinogram system with closed-cycle helium recondensing. *IEEE Trans Appl Supercond* 2017;27(4):1–4.
- Aizawa T, Sato T, Sasaki H, Matsumoto F, Morozumi N, Kusakabe T, Itoi E, Kokubun S. Results of surgical treatment for thoracic myelopathy: minimum 2-year follow-up study in 132 patients. *J Neurosurg Spine* 2007;7(1):13–20.
- Cracco RQ. Spinal evoked response: Peripheral nerve stimulation in man. *Electroencephalogr Clin Neurophysiol* 1973;35(4):379–86.
- Desmedt JE, Cheron G. Spinal and far-field components of human somatosensory evoked potentials to posterior tibial nerve stimulation analysed with oesophageal derivations and non-cephalic reference recording. *Electroencephalogr Clin Neurophysiol* 1983;56(6):635–51.
- el-Negamy E, Sedgwick EM. Properties of a spinal somatosensory evoked potential recorded in man. *J Neurol Neurosurg Psychiatry* 1978;41(8):762–8.
- Fukuoka Y, Komori H, Kawabata S, Ohkubo H, Shinomiya K. Visualization of incomplete conduction block by neuromagnetic recording. *Clin Neurophysiol* 2004;115(9):2113–22.
- Fukuoka Y, Komori H, Kawabata S, Ohkubo H, Shinomiya K, Terasaki O. Imaging of neural conduction block by neuromagnetic recording. *Clin Neurophysiol* 2002;113(12):1985–92.
- Hoshino Y, Kawabata S, Komori H, Ohkubo H, Tomizawa M, Shinomiya K. Three-dimensional neuromagnetic recording in the spinal cord. *Int Congr Ser* 2005;1278:309–12.
- Hsieh P-C, Lee S-T, Chen J-F. Lower thoracic degenerative spondylolisthesis with concomitant lumbar spondylosis. *Clin Neurol Neurosurg* 2014;118:21–5.
- Ishii S, Kawabata S, Tomizawa S, Tomori M, Sakaki K, Shinomiya K, et al. Conductive neuromagnetic fields in the lumbar spinal canal. *Clin Neurophysiol* 2012;123(8):1656–61.

- Jones SJ, Edgar MA, Ransford AO. Sensory nerve conduction in the human spinal cord: epidural recordings made during scoliosis surgery. *J Neurol Neurosurg Psychiatry* 1982;45(5):446–51.
- Kakigi R, Shibasaki H, Hashizume A, Kuroiwa Y. Short latency somatosensory evoked spinal and scalp-recorded potentials following posterior tibial nerve stimulation in man. *Electroencephalogr Clin Neurophysiol* 1982;53(6):602–11.
- Kato F, Yukawa Y, Suda K, Yamagata M, Ueta T. Normal morphology, age-related changes and abnormal findings of the cervical spine. Part II: Magnetic resonance imaging of over 1,200 asymptomatic subjects. *Eur Spine J* 2012;21(8):1499–507.
- Kawabata S, Komori H, Mochida K, Harunobu O, Shinomiya K. Visualization of conductive spinal cord activity using a biomagnetometer. *Spine (Phila Pa 1976)* 2002;27(5):475–9.
- Kumihashi I, Sekihara K. Array-gain constraint minimum-norm spatial filter with recursively updated gram matrix for biomagnetic source imaging. *IEEE Trans Biomed Eng* 2010;57(6):1358–65.
- Lloyd DP, McIntyre. Dorsal column conduction of group I muscle afferent impulses and their relay through Clarke's column. *J Neurophysiol* 1950;13(1):39–54.
- Maccabee Paul J, Levine David B, Pinkhasov Elizabeth I, Cracco Roger Q, Tsairis Peter. Evoked potentials recorded from scalp and spinous processes during spinal column surgery. *Electroencephalogr Clin Neurophysiol* 1983;56(6):569–82.
- Macon JB, Poletti CE. Conducted somatosensory evoked potentials during spinal surgery. Part 1: control conduction velocity measurements. *J Neurosurg* 1982;57(3):349–53.
- Matsumoto M, Fujimura Y, Suzuki N, Nishi Y, Nakamura M, Yabe Y, Shiga H. MRI of cervical intervertebral discs in asymptomatic subjects. *J Bone Joint Surg Br* 1998;80-B(1):19–24.
- Matsuyama Y, Yoshihara H, Tsuji T, Sakai Y, Yukawa Y, Nakamura H, et al. Surgical outcome of ossification of the posterior longitudinal ligament (OPLL) of the thoracic spine: implication of the type of ossification and surgical options. *J Spinal Disord Tech* 2005;18(6):492–7. discussion 8.
- Noble D. Applications of Hodgkin-Huxley equations to excitable tissues. *Physiol Rev* 1966;46(1):1–50.
- Ohkubo H, Komori H, Kawabata S, Fukuoka Y, Shinomiya K. Estimation of localization of neural activity in the spinal cord using a biomagnetometer. *J Med Dent Sci* 2003;50(2):177–82.
- Onishi E, Yasuda T, Yamamoto H, Iwaki K, Ota S. Outcomes of surgical treatment for thoracic myelopathy: a single-institutional study of 73 patients. *Spine (Phila Pa 1976)* 2016;41(22):E1356–63.
- Sakaki K, Hoshino Y, Kawabata S, Adachi Y, Watanabe T, Sekihara K, et al. Evaluation of neural activity by magnetospinography with 3D sensors. *Clin Neurophysiol* 2020;131(6):1252–66.
- Schiff JA, Cracco RQ, Rossini PM, Cracco JB. Spine and scalp somatosensory evoked potentials in normal subjects and patients with spinal cord disease: Evaluation of afferent transmission. *Electroencephalogr Clin Neurophysiol* 1984;59(5):374–87.
- Sekihara K, Kawabata Y, Ushio S, Sumiya S, Kawabata S, Adachi Y, et al. Dual signal subspace projection (DSSP): a novel algorithm for removing large interference in biomagnetic measurements. *J Neural Eng* 2016;13(3):036007.
- Sekihara K, Nagarajan SS. *Electromagnetic Brain Imaging*. Cham: Springer International Publishing: a Bayesian perspective; 2015.
- Shields LBE, Iyer VG, Zhang YP, Shields CB. Missed thoracic myelopathy: Do not throw the hammer away yet. *Surg Neurol Int* 2019;10:158.
- Shinomiya K, Furuya K, Sato R, Okamoto A, Kurosa Y, Fuchioka M. Electrophysiologic diagnosis of cervical OPLL myelopathy using evoked spinal cord potentials. *Spine (Phila Pa 1976)* 1988;13(11):1225–33.
- Sumiya S, Kawabata S, Hoshino Y, Adachi Y, Sekihara K, Tomizawa S, et al. Magnetospinography visualizes electrophysiological activity in the cervical spinal cord. *Sci Rep* 2017;7(1):2192.
- Tani T, Ishida K, Ushida T, Yamamoto H. Intraoperative electroneurography in the assessment of the level of operation for cervical spondylotic myelopathy in the elderly. *J Bone Joint Surg Br* 2000;82(2):269–74.
- Tomizawa S, Kawabata S, Komori H, Hoshino Fukuoka Y, Shinomiya K. Evaluation of segmental spinal cord evoked magnetic fields after sciatic nerve stimulation. *Clin Neurophysiol* 2008;119(5):1111–8.
- Tomori M, Kawabata S, Tomizawa S, Ishii S, Enomoto M, Adachi Y, et al. Diagnosis of incomplete conduction block of spinal cord from skin surface using spinal cord evoked magnetic fields. *J Orthop Sci* 2010;15(3):371–80.
- Trahms L, Erné SN, Trontelj Z, Curio G, Aust P. Biomagnetic functional localization of a peripheral nerve in man. *Biophys J* 1989;55(6):1145–53.
- Ushio S, Hoshino Y, Kawabata S, Adachi Y, Sekihara K, Sumiya S, et al. Visualization of the electrical activity of the cauda equina using a magnetospinography system in healthy subjects. *Clin Neurophysiol* 2019;130(1):1–11.
- Wijesinghe RS. Magnetic measurements of peripheral nerve function using a neuromagnetic current probe. *Exp Biol Med (Maywood)* 2010;235(2):159–69.
- Yamada T, Machida M, Kimura J. Far-field somatosensory evoked potentials after stimulation of the tibial nerve. *Neurology* 1982;32(10):1151–8.